UNCLASSIFIED

SECURITY CLASSIFICATION OF THIS PAGE (When Data Entered)

REPORT DOCUMENTATION PAGE	READ INSTRUCTIONS BEFORE COMPLETING FORM
1. REPORT NUMBER: ARCSL-TR-81001 ✓	2. GOVT ACCESSION NO.: AD-A100 713
3. RECIPIENT'S CATALOG NUMBER	
4. TITLE (and Subtitle): A MATHEMATICAL MODEL OF THE PROBABILITY OF PERFORATION OF THE HUMAN SKULL BY A BALLISTIC PROJECTILE	5. TYPE OF REPORT & PERIOD COVERED: Technical Report, October 1978 - August 1980
	6. PERFORMING ORG. REPORT NUMBER
7. AUTHOR(s): Larry M. Sturdivan and Roy Bexon*	8. CONTRACT OR GRANT NUMBER(s)
9. PERFORMING ORGANIZATION NAME AND ADDRESS: Commander/Director, Chemical Systems Laboratory, ATTN: DRDAR-CLB-P, Aberdeen Proving Ground, Maryland 21010	10. PROGRAM ELEMENT, PROJECT, TASK AREA & WORK UNIT NUMBERS: Project 1L162622 A554
11. CONTROLLING OFFICE NAME AND ADDRESS: Commander/Director, Chemical Systems Laboratory, ATTN: DRDAR-CLJ-R, Aberdeen Proving Ground, Maryland 21010	12. REPORT DATE: April 1981
	13. NUMBER OF PAGES: 29
14. MONITORING AGENCY NAME & ADDRESS(if different from Controlling Office)	15. SECURITY CLASS. (of this report): UNCLASSIFIED
	15a. DECLASSIFICATION/DOWNGRADING SCHEDULE: NA

16. DISTRIBUTION STATEMENT (of this Report)

Approved for public release; distribution unlimited.

17. DISTRIBUTION STATEMENT (of the abstract entered in Block 20, if different from Report)

18. SUPPLEMENTARY NOTES

* Chemical Defense Establishment, Porton Down, Salisbury, WILTS, UK. This report is the first of several produced during a 2-year exchange of personnel between CDE and CSL under TTCP Panel W1. It is published in the UK as CDE Technical Paper No 269.

19. KEY WORDS (Continue on reverse side if necessary and identify by block number)

Penetration	Mathematical model	Projectile	Probability model
Perforation	Logistic function	Cube	Cratering
Skull	Ballistics	Sphere	Forensic pathology
Model	Wound ballistics	Fragment	Presented area

20. ABSTRACT (Continue on reverse side if necessary and identify by block number)

A mathematical model for the probability of penetration of the unprotected human skull is presented which relates the energy of the projectile to the properties of the skull. The model is specifically for steel spheres and cubes but can be used for other projectile shapes or densities provided that care is taken. Constants are obtained for the probabilistic model which allow calculation of the probability of penetration or, conversely, the velocity for a given probability of penetration for a given projectile/skull thickness combination.

DD FORM 1 JAN 73 1473 EDITION OF 1 NOV 65 IS OBSOLETE

UNCLASSIFIED

SECURITY CLASSIFICATION OF THIS PAGE (When Data Entered)

PREFACE

The work described in this report was authorized under Project 1L1622 A554, Bioresponse to Trauma. It was conducted under a scientific exchange program, sponsored by The Technical Cooperation Program, Panel W1, during the period October 1978 through August 1980.

This report is published in the UK as CDE Technical Paper No 269.

CONTENTS

LIST OF SYMBOLS

Symbol	Representing	Units
A	mean presented area of projectile area of top of truncated cone	cm^2
a,b	constants in logistic function	
d	tensile elastic limit of skull	cm
D	$2\sqrt{A/\pi}$ (diameter of sphere of same mean presented area)	cm
m	mass of projectile	kg
P	probability of penetration of skull	
r	radius of top surface of truncated cone (main text) polar co-ordinate (Appendix A)	cm
R	radius of base of truncated cone	cm
s	length of side of cone	cm
S	surface area of the side of the cone	cm^2
t	mean thickness of skull under area of impact	cm
T	tensile strength of skull	$N\ cm^{-2}$
v	velocity of projectile	$m\ s^{-1}$
v_{50}	velocity at which there is a 50% chance of skull penetration	$m\ s^{-1}$
X	model variable (defined in equation 4)	
X_{50}	model variable corresponding to v_{50} (= exp(-a/b))	
Ψ	half angle of the truncated cone	degrees
θ	polar co-ordinate (Appendix A)	degrees
ϕ	polar co-ordinate (Appendix A)	degrees

A MATHEMATICAL MODEL OF THE PROBABILITY OF PERFORATION OF THE HUMAN SKULL BY A BALLISTIC PROJECTILE

1. INTRODUCTION

In civilian, as well as military environments, there are sometimes hazards from ballistic fragments. Because of the extreme vulnerability of the brain to penetrating injury, the difference between a relatively harmless wound and a lethal one often hinges on whether the skull is perforated when struck by one of these projectiles. In the military application, an important part of determining the vulnerability of the soldier or, conversely, the effectiveness of protective helmets lies in our ability to predict the circumstances under which the skull will withstand the impact of a fragment or bullet. In this report a mathematical model is developed which provides an estimate of the probability of perforation of the inner table of the skull and subsequent penetration of the brain by a cube or sphere. This probability is considered a function of the striking velocity and other physical properties of the projectile as well as the thickness of the bone under the impact area.

2. DERIVATION OF THE MODEL

The skull is composed of inner and outer surfaces of hard compact bone and an area between, called cancellous bone, which is less dense because it contains a higher percentage of living cells. The impacting projectile, when it perforates, punches out a hole in the outer table roughly its own size. The area over which the force is exerted spreads within the cancellous portion, causing a larger and more irregular hole in the inner table. This phenomenon is often called "cratering" and is used by forensic pathologists to tell exit from entrance wounds in the skull. This is possible because the larger, irregular hole is in the outer table with an exit wound.

To simplify the mathematical model, this phenomenon is idealized by the following assumptions:

1. In the region of the impact the skull is a flat homogeneous plate of bone with uniform mechanical properties.

2. When the skull is perforated by a projectile, a truncated right circular cone of bone is driven out in front of the fragment.

3. The top of the truncated cone has an area equal to the mean presented area of the projectile; i.e., the projectile orientation is assumed to be random.

4. The velocity of sound in bone is much greater than the velocity of perforation, so compressional effects may be neglected.

5. The probability of perforation depends only on the logarithm of the ratio of the stress imposed on the skull by the impacting projectile to the tensile strength of the bone.

6. The underlying probability distribution governing perforation is well approximated by the logistic distribution on the model variable, the log stress ratio of assumption 5 (e.g., if the true distribution were Gaussian this assumption would be valid). Some of the factors contributing to the variance of the probability distribution are variations in the mechanical properties of bone from skull

to skull, differences in the proportion of cortical to cancellous bone, and random deviations from some of the assumptions listed above (for instance, deviation from conical shape in the crater), each of which is unique.

A schematic diagram of the penetrating projectile is shown in figure 1. For purposes of illustration, the projectile is idealized as a right circular cylinder impacting end-on. The terms which will be used in developing the model, most of which appear in figure 1, are defined in the list of symbols. The units used are not SI but are those customarily used in wound ballistics and are retained here as a matter of convenience.

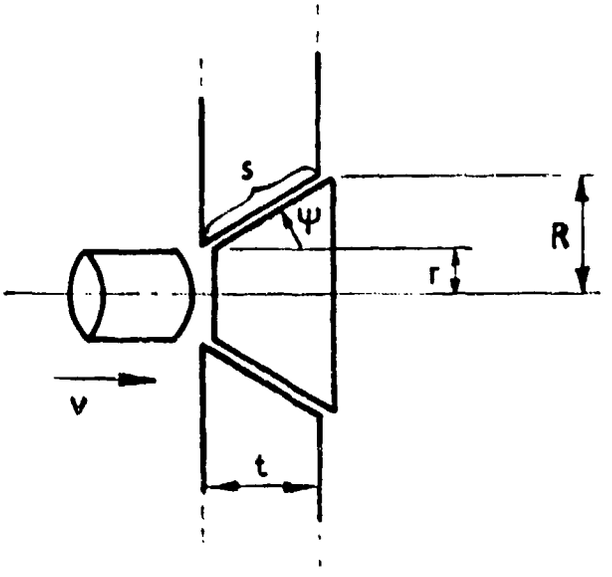

Figure 1. Idealized Schematic Diagram of Cylinder Perforating Skull

The surface area of the side of the truncated cone is given by:

$$S = \pi (r + R)s \tag{1}$$

But $s = t \sec\Psi$ and $R = r + t \tan\Psi$, so

$$S = \pi (2r + t \tan\Psi)t \sec\Psi \tag{2}$$

The minimum average force exerted in pushing out the conical section of skull may be approximated by dividing the kinetic energy of the projectile by the hypothetical elastic limit of the bone, i.e., the distance that the plug could be moved before it would break loose from the surrounding material. Thus,

$$\text{force} \approx \tfrac{1}{2}mv^2/d$$

$$\text{tensile stress} \approx \text{force}/S$$

$$\text{stress ratio} = \text{tensile stress/tensile strength } (T)$$

$$= \frac{\tfrac{1}{2}\, mv^2/d}{T\,\pi\,(2r + t\ \tan)t\ \sec\Psi} \tag{3}$$

The quantity 2r may be replaced by the variable $D = 2\sqrt{A/\pi}$ to generalize to a projectile with a noncircular presented area. When inserted into the probability function, the multiplicative constants of equation 3 may be absorbed into logistic parameter a (see equation 5 below). With these modifications the stress ratio becomes the model variable,

$$X = \frac{\tfrac{1}{2}\, mv^2}{t^2\sec\Psi(D/t + \tan\Psi)} = \frac{\tfrac{1}{2}\, mv^2/t^2 \quad *}{\sec\Psi(D/t + \tan\Psi)} \tag{4}$$

We will use the logistic probability distribution function to estimate the probability of penetration of the skull,

$$P = \frac{1}{1 + e^{-(a + b\ln X)}} \tag{5}$$

where a and b are determined from data (see next section).

The natural logarithm (ln) of X is used instead of X itself to equalize the variance over the domain of definition. This requirement is most easily explained by use of an example: Suppose we are concerned with the probability that a certian projectile will perforate some material in sheets of different thicknesses where the probability of perforation is a function of velocity alone. On a thin sheet where the v_{50}, the velocity at which the probability of perforation is 0.5, is 100 m/s, we would expect a standard deviation on the order of tens of meters per second. On a much thicker sheet, where the v_{50} is 1000 m/s, we no longer expect the standard deviation to be measured in tens, but in hundreds of meters per second. In other words, we expect the standard deviation to be roughly proportional to the magnitude of the mean. In this case, the variance may be approximately equalized over the whole domain by dealing with the logarithms of the numbers rather than with the numbers themselves.

* The equation is expressed in this manner as an aid to plotting X at a later stage.

3. FITTING THE MODEL

The data used were obtained from two previous studies on skull penetration.*,** Since the analysis on these studies showed that the response of dried skulls was significantly different from that of fresh skullcaps, only the latter were used in determining the parameters a and b for the logistic function of equation 5. The physical properties of the five projectiles used are listed in the table.

Table. Projectiles Studied (All Made of Steel)

Projectile	Mass	Mean dimension*	Mean presented area**
	gm	cm	cm^2
0.85 grain sphere	0.055	0.238	0.0445
2.1 grain cube	0.135	0.265	0.1050
4.2 grain cube	0.274	0.333	0.1660
16 grain cube	1.029	0.514	0.3966
225 grain cube	14.694	1.236	2.2933

* Diameter for sphere; edge for cubes.
** Surface area/4; see appendix A.

The ability of the model to properly scale the probability of perforation of skulls of different thickness by projectiles of different mass was tested against the v_{50} of the above five projectiles. The v_{50} was obtained by averaging the five highest nonperforating velocities and the five lowest perforating velocities for each skull thickness for which there were sufficient data.† These data are shown plotted in terms of the model in figure 2. Note that the abscissa is the logarithm of the numerator of the model variable of equation 4, while the ordinate is the logarithm of the denominator. A straight line of slope 1 represents a constant ratio of the numerator and denominator (see appendix B). When drawn through the data in figure 2, this line allows a visual assessment of the goodness of fit of the data from low energy to high energy. The energies are $\frac{1}{2} mv^2_{50}$ for all v_{50} points. Since Ψ is a variable, it may be adjusted to cause the sphere and cube data to be on a common line. A Ψ of 23° for the sphere and 30° for the cubes not only superimposed the two groups but tilted the individual data sets to form the best straight line of slope 1. Since the colinearity of the data with the reference line is relatively insensitive to Ψ, the difference (7° between spheres and cubes) is more significant than the magnitude of Ψ.

* Miller, J. F., Ashman, W. P., and Jameson, J. W. Edgewood Arsenal Technical Report EATR 4373, Ballistic Limits of Skulls Against Steel Cubes, April 1970.
** Mickiewicz, A. P. Chemical Systems Laboratory. Private communication.
† To obtain the maximum number of v_{50} points, a few were averages of 4 and 4 instead of 5 and 5.

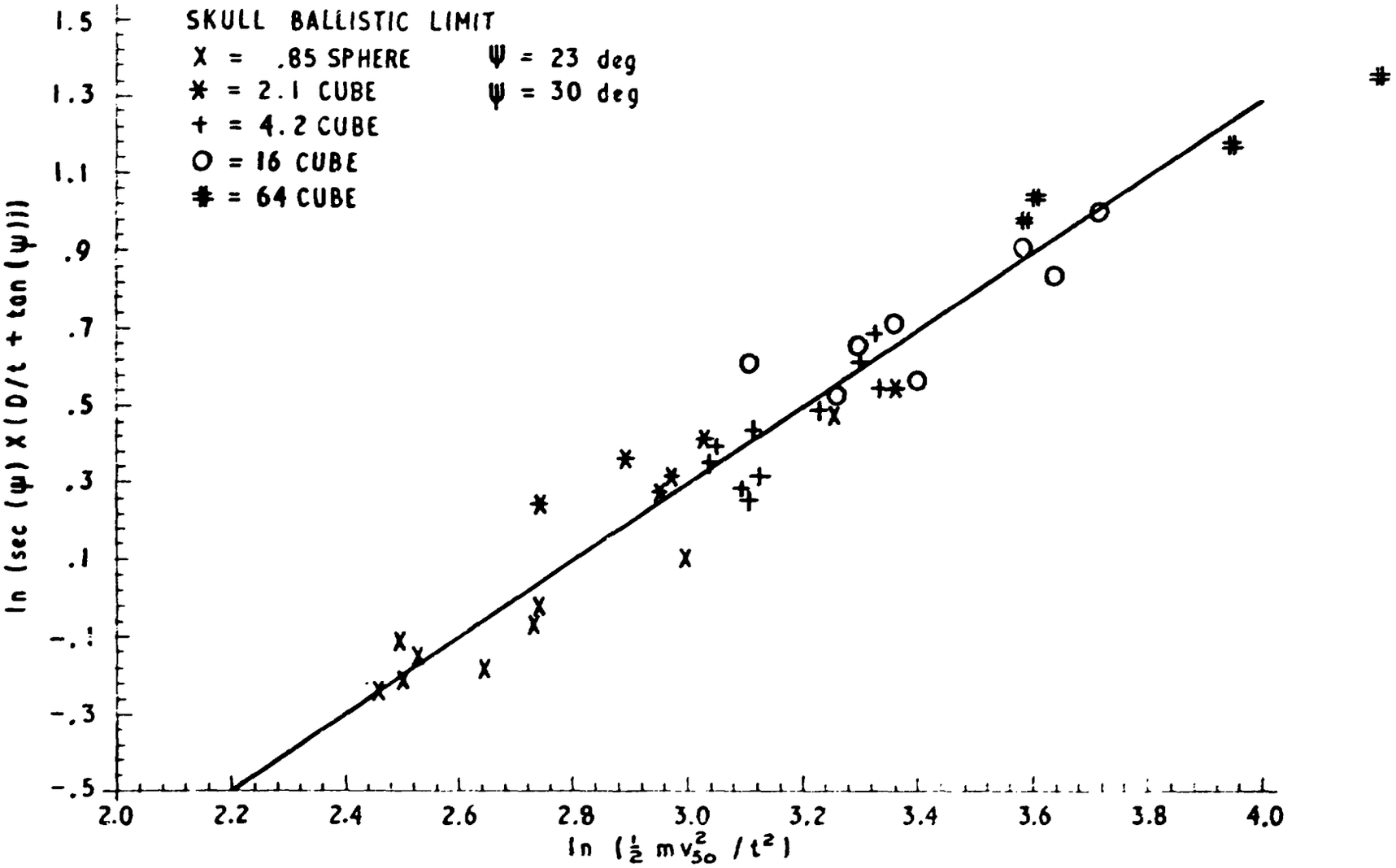

Figure 2. Plot of the Two Components of the Model Variable X With V_{50} Line

After the determination of Ψ, all the variables in equation 4 are known. It is then possible to fit the dichotomous data (perforation or nonperforation) to the logistic function by the approximate least squares method of Walker and Duncan.* In this technique all data are used to approximate the v_{50} for each skull thickness/projectile combination. For each shot the mass, striking velocity, Ψ, skull thickness, and mean presented area are used to calculate X from equation 4. A second number is associated with this value: 1 for perforation, 0 for nonperforation. The Walker-Duncan method then iteratively converges on values of a and b which approximately minimize the sum of squared differences between the predicted probability of penetration (equation 5) and the assigned value (0 to 1) for all shots by all projectiles. The resulting values of a and b are:

$$a = -13.035,\ b = 4.793$$

Lines of slope 1 in figure 2 represent constant values of X and, therefore, discrete levels of probability of perforation. To find the line of 50% probability we insert P = 0.5 in equation 5 and solve.

$$P = \frac{1}{1 + e^{-(a + b\ln X_{50})}} = 0.5$$

or

$$e^{-(a + b\ln X_{50})} = 1$$

This implies

$$a + b\ln X_{50} = 0$$

$$\ln X_{50} = \ln \frac{\frac{1}{2} m v_{50}^2}{t^2 \sec\Psi(D/t + \tan\Psi)} = -a/b \qquad (6)$$

where X_{50} is from equation 4 with $v = v_{50}$.

Therefore,

$$\ln[t^2 \sec\Psi(D/t + \tan\Psi)] = a/b + \ln[\tfrac{1}{2} m v_{50}^2] \qquad (7)$$

It is this line which is drawn in figure 2. The good agreement between the line, derived from all data, and the plotted points, derived from a few selected data points, lend some credence to the validity of using those approximate v_{50} points in determining the value of Ψ. An example of the use of the model is given in appendix C.

* Walker, S. H., and Duncan, D. B. Estimation of the Probability of an Event as a Function of Several Independent Variables. Biometrika *54*, 167-179 (1967).

4. SUMMARY AND CONCLUSIONS

The model derived above is based on the assumption that a plug of homogeneous material in the shape of a truncated cone is driven out of the skull by the perforating projectile. The area of the small end of the truncated cone is assumed equal to the mean presented area of the projectile. Under these assumptions, both spheres and cubes may be accommodated in the same model by letting the half angle of the cone take on different values for the two shapes. Experience with previous models of penetration has shown that chunky, irregular fragments usually behave in a manner more similar to cubes than spheres. Therefore, it was suggested that the cube half angle, $\Psi = 30°$, be used for fragments as well.

The data used in fitting this model were obtained from impacts on bare bone. In predicting the probability of penetrating the skull of live humans, this model neglects the protection offered by the scalp and (sometimes) hair. Thus the model is conservative in the sense of predicting somewhat higher probabilities of penetration that would actually be observed in live human skulls of the same thickness.

Caution must be exercised when applying these criteria to projectiles larger than those in the data base or of density much different from that of steel. There are no data available to test the model outside the range of masses and presented areas of the projectiles of the table. Large projectiles at lower velocities are particularly risky because of significant curvature of the skull over large areas and different mechanisms of skull fracture which occur under these conditions. It should also be noted that assumption 3 requires random orientation of the impacting projectile. This will be valid for projectiles whose mean dimension is not much larger than the thickness of the skull, since in perforating the skull the projectile will ultimately present its mean area, e.g., by rotation during penetration. For projectiles whose mean dimension is greater than the skull thickness (for example, paper weights), the projectile is unlikely to perforate presenting its mean area, and the effect of orientation of the projectile will be important.

5. RECOMMENDATIONS FOR FURTHER WORK

When examining the skullcaps perforated by cubes, one does not see flat-sided holes with neat square corners, but rounded holes. This indicates that the assumption of equality between the mean presented area of the projectile and the area of the hole in the outer table should instead be an assumption of proportionality. Differences between spheres and cubes could then be accounted for by different constants of proportionality rather than different half angles Ψ. Irregular fragments would have a proportionality constant somewhere between those of the cube and sphere. Unfortunately, there are no data available for irregular fragments nor even sufficient data for the spheres and cubes to allow an accurate determination of the proportionality constants.

If additional data are acquired, particularly fragment data, it is suggested that the following model be tried:

$$X = \frac{\frac{1}{2} mv^2}{t(kD + t \tan\Psi)}$$

where k depends on the shape of the projectile (sphere, cube, chunky fragment, etc.) and Ψ is a constant, independent of shape.

APPENDIX A

MEAN PRESENTED AREA

Let us first develop the "simple case" of the mean presented area of a sphere. We want to express this as a fraction of its total surface area. To obtain the surface area we will integrate in polar co-ordinates as in figure A-1. Notice that the width of the element of area dA is r sin θ dϕ. The sine function is necessary because, like the outer surface of an orange segment, it must narrow to a point at the top (θ = 0). Even if the wedge is infinitesimally thin, it still must be shaped like a wedge. Another way of looking at this effect is to imagine θ held constant; then when we rotate around the vertical (z) axis through an angle dϕ, the distance moved on the surface is r sin θ dϕ. The surface area of the sphere is

$$A_S = \int_0^{2\pi}\int_0^{\pi} r^2 \sin\theta \, d\theta \, d\phi = r^2 \int_0^{2\pi} (-\cos\theta) \Big|_0^{\pi} d\phi \qquad (A\text{-}1)$$

$$= 2r^2 \int_0^{\pi} d\phi = 4\pi r^2$$

Referring again to figure A-1, we now wish to obtain the mean area projected on the plane P1 at the right of the figure, parallel to the x-z plane. The width and height of dA as projected on this plane are r sinθ sinϕ dϕ and r sinθ dθ. Thus the projected area is

$$A_P = \int_0^{\pi}\int_0^{\pi} r^2 \sin\phi \sin^2\theta \, d\theta \, d\phi \qquad (A\text{-}2)$$

where the limits of integration on ϕ are 0 and π because the region from π to 2π is on the far side of the sphere from the plane P1 and does not contribute to the presented area required. Thus,

$$A_P = r^2 \int_0^{\pi} \sin\phi \left[\frac{\theta}{2} - \frac{1}{4}\sin 2\theta\right]_0^{\pi} d\phi$$

$$= \frac{\pi r^2}{2} \int_0^{\pi} \sin\phi \, d\phi = \pi r^2 \qquad (A\text{-}3)$$

The mean presented area A_P (as expected) is the same as the cross-sectional area and is a quarter of the surface area. The angles θ and ϕ may be interchanged without affecting the results.

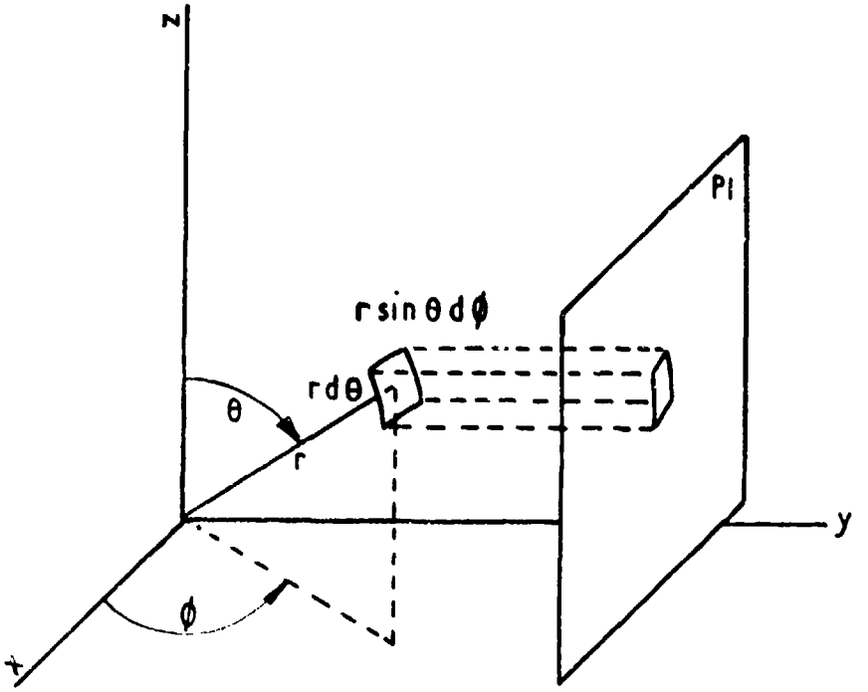

Figure A-1. Element of Area of a Sphere and
Its Projection on a Plane

We now turn to the problem of the mean presented area of a polyhedron with an arbitrary number q of plane elements as its surface. Let the area of a typical element be E. Then the projected area of the element E, under all possible orientations of the polyhedron with respect to the plane of projection (x-z), is equivalent to the projected area of E rotated about its center of mass as in figure A-2. The co-ordinate system is centered at the center of mass in such a way that the normal $\underline{n}$ to the area E makes an angle θ with the z-axis. The projection of the normal onto the x-y plane makes an angle ϕ with the x-axis. The integral of the area projected onto P1 is

$$A_I = E \int_0^{\pi} \int_0^{\pi} \sin\theta \, \sin\phi \, d\phi \, \sin\theta \, d\theta \qquad \text{(A-4)}$$

$$= E \int_0^{\pi} \int_0^{\pi} \sin\phi \, \sin^2\theta \, d\theta \, d\phi = \pi E$$

where the first $\sin\theta$ is, as above, necessary to provide equal weight to all possible orientations. Because E is a finite area (not an infinitesimal), the area A_I is an integral projected area - not a mean. To obtain the mean, we must divide A_I by the total solid angle subtended by all possible orientations of the element E (i.e., the solid angle swept out by $\underline{n}$), namely 4π. Thus the mean projected area $A_P = A_I/4\pi = E/4$.

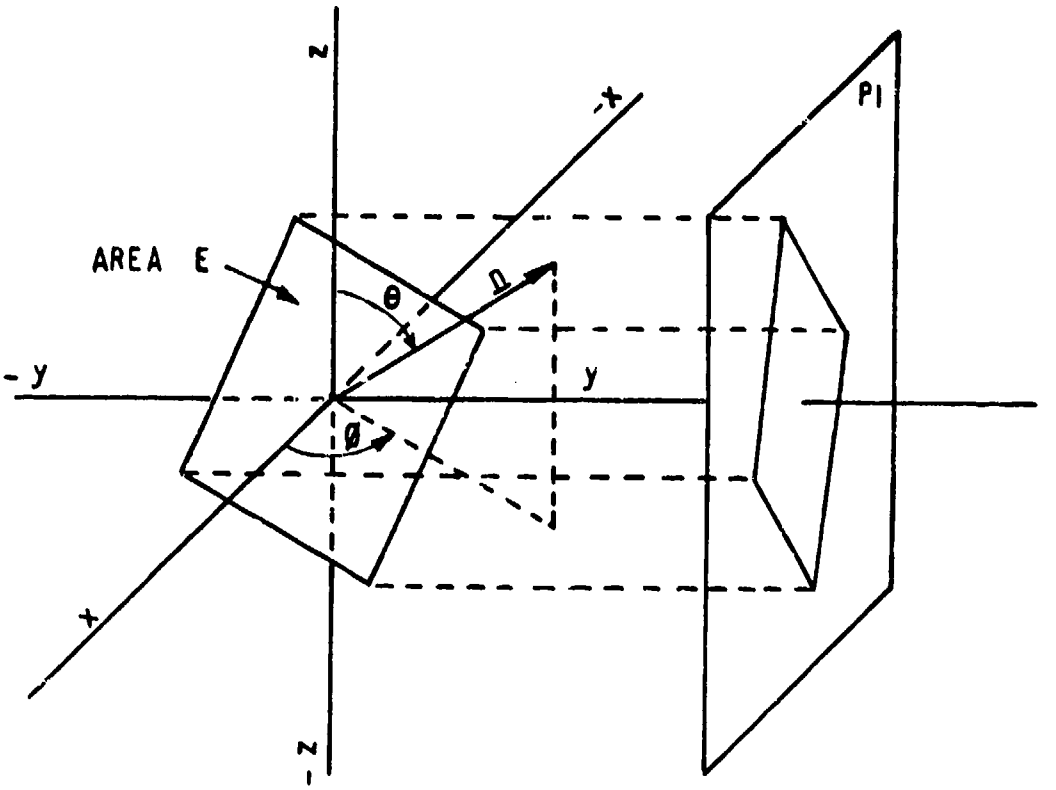

Figure A-2. Element of Area of a Polyhedron
and Its Projection on a Plane

If there are q elemental areas in the polyhedron each having a mean projected area equal to a quarter of its surface area, the total mean projected area is a quarter of the total surface area, i.e.,

$$A_P = \sum_{i=1}^{q} A_i/4 = \frac{1}{4} \sum_{i=1}^{q} A_i = \frac{1}{4} A_S \qquad \text{(A-5)}$$

This formula is valid for convex surfaces only. If there were a concave portion on the surface, it would be shielded by another part of the surface on part of the interval $0\text{-}\pi$ of one or both angles of equation A-4. Any convex shape can be approximated to any specified accuracy by making q sufficiently large and the A_i sufficiently small. Thus the mean presented area of a convex solid is $\frac{1}{4}$ of its total surface area.

APPENDIX B

COMMENTS ON THE SLOPE OF A LOG - LOG PLOT

Consider the graph in the figure, where the two variables N and D are plotted on logarithmic axes. Suppose the data indicate a straight line relationship on this graph.

Then,

$$\ln D = p \ln N + q$$

$$= \ln N^p + q$$

$$\therefore \ln N^p - \ln D = -q$$

$$\therefore \ln\left(\frac{N^p}{D}\right) = -q$$

$\therefore$ after exponentiating,

$$\frac{N^p}{D} = e^{-q} = \frac{1}{q'}$$

If $p = 1$, there is a constant ratio between N and D.

If $p = 2$, there is a constant ratio between N^2 and D.

If $N = \frac{1}{2}mv^2/t^2$ and $D = \sec\Psi(D/t + \tan\Psi)$ the $N/D = X$ (see equation 4). A line of slope 1 in the plot of ln N v ln D then represents a constant ratio between $\frac{1}{2}mv^2/t^2$ and $\sec\Psi(D/t + \tan\Psi)$.

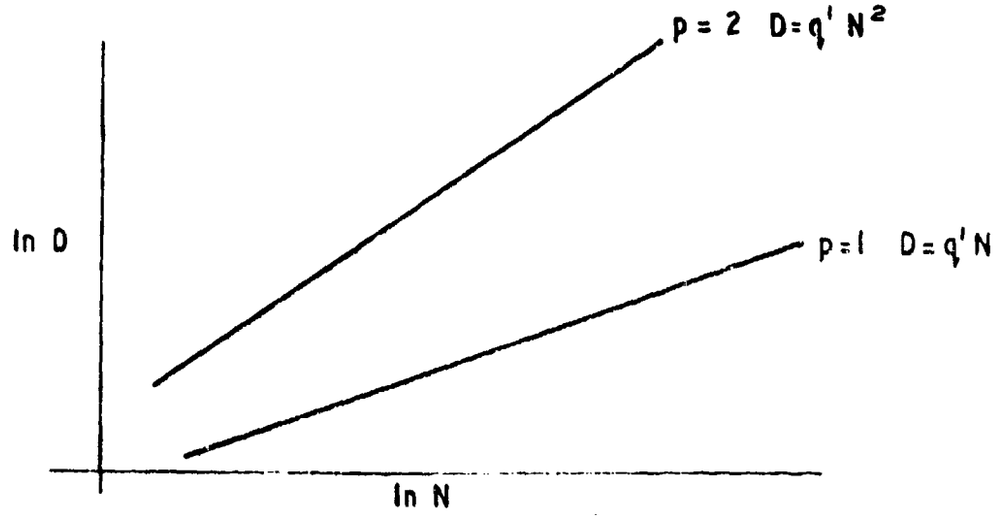

Figure. General Linear Relationship Between ln N and ln D

APPENDIX C

EXAMPLE OF THE USE OF THE MATHEMATICAL MODEL

Let us assume that we wish to know the velocity corresponding to a 0.5 probability of penetration for a 0.5-gram cube of mean presented area 0.245 cm^2 impacting a skull of 0.5-cm thickness. From equation 6 we obtain

$$v_{50} = |2t^2 \sec\Psi(D/t + \tan\Psi)\exp(-a/b)/m|^{1/2}$$

where

$$D = 2\sqrt{A/\pi} = 2\sqrt{0.245/\pi} = 0.5585 \text{ cm}$$

$$\Psi = 30°$$

$$t = 0.5 \text{ cm}$$

$$m = 0.0005 \text{ kg}$$

$$a = -13.035$$

$$b = 4.793$$

Substitution above gives v_{50} = 172 m/s. Suppose we wish to know the probability of penetrating the skull if the cube of our example impacts at 200 m/s. From equation 4 we obtain

$$X = \frac{\frac{1}{2} mv^2}{t^2 \sec\Psi(D/t + \tan\Psi)} = 20.44$$

Then

$$P = \frac{1}{1 + \exp(-a - b\ln X)} = 0.807$$

The following table can be constructed using similar calculations, assuming the same fragment and skull thickness:

Velocity m/s	Probability of penetration
150	0.209
175	0.537
200	0.807
225	0.973

The value of probability of penetration above does not indicate the proportion of the skull thickness penetrated but rather the proportion of hits which would be expected to punch out a plug of bone

from the skull given a large number of hits. Thus, in the example above, at v = 200 m/s, 80.7% of all shots fired would be expected to penetrate for that fragment/skull thickness combination, while 19.3% would not. No attempt is made to predict the outcome of individual shots.

DISTRIBUTION LIST 11

Names	Copies
CHEMICAL SYSTEMS LABORATORY	
ATTN: DRDAR-CLF	1
ATTN: DRDAR-CLC-B	1
ATTN: DRDAR-CLC-C	1
ATTN: DRDAR-CLC-E	1
ATTN: DRDAR-CLJ-R	3
ATTN: DRDAR-CLJ-L	3
ATTN: DRDAR-J-M	1
ATTN: DRDAR-CLJ-P	1
ATTN: DRDAR-CLT	1
ATTN: DRDAR-CLT-E	1
ATTN: DRDAR-CLT-P	1
ATTN: DRDAR-CLN	1
ATTN: DRDAR-CLW	1
ATTN: DRDAR-CLW-C	1
ATTN: DRDAR-CLW-P	1
ATTN: DRDAR-CLW-E	1
ATTN: DRDAR-CLB-C	1
ATTN: DRDAR-CLB-P	1
ATTN: DRDAR-CLB-PA	1
ATTN: DRDAR-CLB-PO	1
ATTN: DRDAR-CLB-R	1
ATTN: DRDAR-CLB-T	1
ATTN: DRDAR-CLB-TE	1
ATTN: DRDAR-CLY-A	1
ATTN: DRDAR-CLY-R	6
ATTN: DRDAR-CLR-I	1
COPIES FOR AUTHOR(S): Research Division	12
DEPARTMENT OF DEFENSE	
Defense Technical Information Center ATTN: DTIC-DDA-2 Cameron Station, Building 5 Alexandria, VA 22314	12
Director Defense Intelligence Agency ATTN: DB-4G1 Washington, DC 20301	1
Special Agent In Charge ARO, 902d Military Intelligence GP ATTN: IAGPA-A-AN Aberdeen Proving Ground, MD 21005	1
Commander SED, HQ, INSCOM ATTN: IRFM-SED (Mr. Joubert) Fort Meade, MD 20755	1
DEPARTMENT OF THE ARMY	
HQDA (DAMO-NCC) WASH DC 20310	1
Federal Emergency Management Agency Office of Mitigation and Research ATTN: David W. Bensen Washington, DC 20472	1
Deputy Chief of Staff f Research, Development & Acquisition ATTN: DAMA-CSS-C ATTN: DAMA-ARZ-D Washington, DC 20310	1 1
Department of the Army Headquarters, Sixth US Army ATTN: AFKC-OP-NBC Presidio of San Francisco, CA 94129	1
US Army Research and Standardization Group (Europe) ATTN: DRXSN-E-SC Box 65, FPO New York 09510	1
HQDA (DAMI-FIT) WASH, DC 20310	1
Commander HQ 7th Medical Command ATTN: AEMPM APO New York 09403	1
Commander DARCOM, STITEUR ATTN: DRXST-ST1 Box 48, AO New York 09710	1
Commander USAOTEA ATTN: CSTE-ZX 5600 Columbia Pike Falls Church, VA 22041	1

Commander
US Army Science & Technology Center-
Far East Office
ATTN: MAJ Borges 1
APO San Francisco 96328

Commander
2d Infantry Division
ATTN: EAIDCOM 1
APO San Francisco 96224

Commander
5th Infantry Division (Mech)
ATTN: Division Chemical Officer 1
Fort Polk, LA 71459

OFFICE OF THE SURGEON GENERAL

Commander
US Army Medical Bioengineering Research
and Development Laboratory
ATTN: SGRD-UBD-AL 1
Fort Detrick, Bldg 568
Frederick, MD 21701

Headquarters
US Army Medical Research and
Development Command
ATTN: SGRD-PL 1
Fort Detrick, MD 21701

Commander
USA Biomedical Laboratory
ATTN: SGRD-UV-L 1
Aberdeen Proving Ground, MD 21010

US ARMY HEALTH SERVICE COMMAND

Superintendent
Academy of Health Sciences
US Army
ATTN: HSA-CDH 1
ATTN: HSA-IPM 1
Fort Sam Houston, TX 78234

US ARMY MATERIEL DEVELOPMENT AND
READINESS COMMAND

Commander
US Army Materiel Development and
Readiness Command
ATTN: DRCLDC 1
ATTN: DRCSF-P 1
5001 Eisenhower Ave
Alexandria, VA 22333

Project Manager Smoke/Obscurants
ATTN: DRCPM-SMK 1
Aberdeen Proving Ground, MD 21005

Director
Human Engineering Laboratory
ATTN: DRXHE-SP (CB Defense Team) 1
Aberdeen Proving Ground, MD 21005

Commander
US Army Foreign Science & Technology
Center
ATTN: DRXST-MT3 1
220 Seventh St., NE
Charlottesville, VA 22901

Director
US Army Materiel Systems Analysis Activity
ATTN: DRXSY-MP 1
ATTN: DRXSY-T (Mr. Metz) 2
Aberdeen Proving Ground, MD 21005

Commander
US Army Missile Command
Redstone Scientific Information Center
ATTN: DRSMI-RPR (Documents) 1
Redstone Arsenal, AL 35809

Director
DARCOM Field Safety Activity
ATTN: DRXOS-C 1
Charlestown, IN 47111

Commander
US Army Natick Research and
Development Command
ATTN: DRDNA-VC 1
ATTN: DRDNA-VCC 1
ATTN: DRDNA-VM 1
ATTN: DRDNA-VR 1
ATTN: DRDNA-VT 1
Natick, MA 01760

US ARMY ARMAMENT RESEARCH AND DEVELOPMENT COMMAND

Commander
US Army Armament Research and Development Command
ATTN: DRDAR-LCA-L 1
ATTN: DRDAR-LCE 1
ATTN: DRDAR-LCE-C 1
ATTN: DRDAR-LCM-E 1
ATTN: DRDAR-LCM-SA 1
ATTN: DRDAR-LCU 1
ATTN: DRDAR-LCU-CE 1
ATTN: DRDAR-PMA (G.R. Sacco) 1
ATTN: DRDAR-SCM 1
ATTN: DRDAR-SCP 1
ATTN: DRDAR-SCA-W 1
ATTN: DRDAR-SER 1
ATTN: DRDAR-TSS 2
ATTN: DRDAR-CAWS-AM 1
ATTN: DRDAR-CAWS-SI 1
Dover, NJ 07801

Director
Ballistic Research Laboratory
ARRADCOM
ATTN: DRDAR-TSB-S 1
Aberdeen Proving Ground, MD 21005

Director
Benet Weapons Laboratory
ATTN: DRDAR-LCB-TL 1
Watervliet, NY 12189

Commander
USA Technical Detachment 1
US Naval EOD Facility
Indian Head, MD 20640

US ARMY ARMAMENT MATERIEL READINESS COMMAND

Commander
US Army Armament Materiel Readiness Command
ATTN: DRSAR-ASN 1
ATTN: DRSAR-IRC 1
ATTN: DRSAR-ISE 1
ATTN: DRSAR-LEP-L 1
ATTN: DRSAR-PDM 1
ATTN: DRSAR-PE 1
ATTN: DRSAR-SF 1
ATTN: DRSAR-SR 1
Rock Island, IL 61299

Commander
USA ARRCOM
ATTN: DRSAR-MAS-C 1
ATTN: DRSAR-MAD-E 1
ATTN: SARTE 1
Aberdeen Proving Ground, MD 21010

Commander
US Army Dugway Proving Ground
ATTN: Technical Library (Docu Sect) 1
Dugway, UT 84022

US ARMY TRAINING & DOCTRINE COMMAND

Commandant
US Army Infantry School
ATTN: NBC Division 1
Fort Benning, GA 31905

Commandant
US Army Missile & Munitions Center and School
ATTN: ATSK-CD-MD 1
ATTN: ATSK-DT-MU-EOD 1
Redstone Arsenal, AL 35809

Commander
US Army Logistics Center
ATTN: ATCL-MG 1
Fort Lee, VA 23801

Commandant
USAMP&CS/TC&FM
ATTN: ATZN-CM-CDM 1
Fort McClellan, AL 36205

Commander
US Army Infantry Center
ATTN: ATSH-CD-MS-C 1
Fort Benning, GA 31905

Commander
US Army Infantry Center
ATTN: ATZB-DPT-PO-NBC 1
Fort Benning, GA 31905

Commander
USA Training and Doctrine Command
ATTN: ATCD-Z 1
Fort Monroe, VA 23651

Commander
USA Combined Arms Center and
Fort Leavenworth
ATTN: ATZL-CA-COG 1
ATTN: ATZL-CAM-IM 1
Fort Leavenworth, KS 66027

Commander
US Army TRADOC System Analysis Activity
ATTN: ATAA-SL 1
White Sands Missile Range, NM 88002

US ARMY TEST & EVALUATION COMMAND

Commander
US Army Test & Evaluation Command
ATTN: DRSTE-CM-F 1
ATTN: DRSTE-CT-T 1
Aberdeen Proving Ground, MD 21005

DEPARTMENT OF THE NAVY

Chief of Naval Research
ATTN: Code 443 1
800 N. Quincy Street
Arlington, VA 22217

Commander
Naval Explosive Ordnance Disposal Facility
ATTN: Army Chemical Officer (Code AC-3) 1
Indian Head, MD 20640

Commander
Naval Surface Weapons Center
White Oak Site
ATTN: Library I-321 1
Silver Spring, MD 20910

Chief, Bureau of Medicine & Surgery
Department of the Navy
ATTN: MED 3C33 1
Washington, DC 20372

Commander
Naval Weapons Center
ATTN: Technical Library (Code 343) 1
China Lake, CA 93555

Commander Officer
Naval Weapons Suport Center
ATTN: Code 5042 (Dr. B.E. Douda) 1
Crane, IN 47522

US MARINE CORPS

Commandant
HQ, US Marine Corps
ATTN: Code LMW 1
Washington, DC 20380

Director, Development Center
Marine Corps Development and
Education Command
ATTN: Fire Power Division 1
Quantico, VA 22134

DEPARTMENT OF THE AIR FORCE

HQ Foreign Technology Division (AFSC)
ATTN: TQTR 1
Wright-Patterson AFB, OH 45433

Commander
Aeronautical Systems Division
ATTN: ASD/AELD 1
ATTN: ASD/AESD
Wright-Patterson AFB, OH 45433

HQ AFLC/LOWMM 1
Wright-Patterson AFB, OH 45433

HQ, AFSC/SDNE 1
Andrews AFB, MD 20334

HQ AMD/RD
ATTN: Chemical Defense OPR 1
Brooks AFB, TX 78235

HQ AFISC/SEV 1
Norton AFB, CA 92409

NORAD Combat Operations Center
ATTN: DOUN 1
Cheyenne Mtn Complex, CO 80914

Air Force Aerospace Medical Research
Laboratory
ATTN: AFAMRL/HE (Dr. C.R. Replogle) 1
Wright-Patterson AFB, OH 45433

USAF SAM/RZW 1
Brooks AFB, TX 78235

HQ AFTEC/SGB 1
Kirtland AFB, NM 87117

OUTSIDE AGENCIES

Battelle, Columbus Laboratories
ATTN: TACTEC 1
505 King Avenue
Columbus, OH 43201

Toxicology Information Center, WG 1008
National Research Council 1
2101 Constitution Ave., NW
Washington, DC 20418

US Public Health Service
Center for Disease Control
ATTN: Lewis Webb, Jr. 1
Building 4, Room 232
Atlanta, GA 30333

Director
Central Intelligence Agency
ATTN: ORD/DD/S&T 1
Washington, DC 20505

ADDITIONAL ADDRESSEES

Commander
US Army Environmental Hygiene Agency
ATTN: Librarian, Bldg 2100 1
Aberdeen Proving Ground, MD 21010

Stimson Library (Documents) 1
Academy of Health Sciences
Bldg. 2840
Fort Sam Houston, TX 78234

Director
Ballistic Research Laboratory
ARRADCOM
ATTN: DRDAR-BLV 1
Aberdeen Proving Ground, MD 21005